Surface Tortuosity and its Application to Analyzing Cracks in Concrete

Tong Zhang , George Nagy
Department of Electrical, Computer, and Systems Engineering
Rensselaer Polytechnic Institute
Troy, NY 1280, USA
E-mail: zhant@rpi.edu, nagy@ecse.rpi.edu

Abstract

Previous studies of tortuosity were restricted to a curve in 2D or 3D. We propose several measures of surface tortuosity based on surface normals and principal curvatures, and apply these measures to analyze the tortuosity of three-dimensional crack surfaces of concrete. We show that all crack surfaces are similar in tortuosity despite their different sizes and locations, while distinctive from various geometric surfaces.

1. Introduction

According to the Oxford English Dictionary, "tortuosity" is the condition of being twisted, crooked, sinuous. Tortuosity is a type of geometrical irregularity. This property has been studied for a curve in 2D or 3D. We have not found studies of this property on a surface.

1.1. Curve Tortuosity

The tortuosity of a curve has been mostly applied to examine the morphology of blood vessels. Normal blood vessels are straight or slightly curved. They become tortuous when diseases such as high blood flow, angiogenesis, and congestion of blood vessels occur. By modeling the blood vessels as curves in 2D or 3D, a measure of tortuosity will enable automatic diagnosis [4, 1].

Tortuosity is also used to measure the diffusion distance of neuro-active molecules in the brain. As the substances confined to the extracellular space diffuse more slowly than in free solution, this study can provide insight into the function of neuro-active molecules [8].

1.2. Motivation

We study the tortuosity of a surface in order to analyze the three-dimensional crack surfaces of concrete. Concrete is a quasi-brittle, heterogeneous material whose fractures are characterized by a wide range of physical processes [9]. Previous research in fracture modeling (a) aimed to understand and predict the bulk fracture response, (b) analyzed the contours of cracks at a low resolution in 2D. However, three-dimensional models are necessary to accurately compute the properties of concrete, which exhibits complex 3D fracture surfaces [2].

With X-ray microtomography, 3D representation of the internal structures of a concrete specimen has been produced at an unprecedented resolution. By applying increasing compressive loads to a specimen, this technique captures the fracture evolution in a sequence of volumetric images [6].

We have developed image processing tools to extract the crack surfaces from these images [10]. Here we discuss measures of surface tortuosity, and apply them to investigate the properties of these cracks.

In Section 2, we review various measures of curve tortuosity in 2D and 3D. We propose new measures of surface tortuosity in Section 3. Section 4 contains the results of these measures on crack surfaces. We summarize our findings in Section 5.

2. Measures of Curve Tortuosity

There are three common measures of curve tortuosity: the distance ratio, the number of inflection points, and the sum of angles.

Distance Ratio: The distance ratio is the easiest and most frequently-used measure. It is defined as the ratio of the length of the curve to the distance between its end points (Figure 1 (a)). The measure can be applied to a curve in either 2D or 3D, but the problem is that it is insensitive to how the curve "wiggles". For example, in Figure 1 (b), the curve of the largest half-circle has the same distance ratio as the curve composed of a series of smaller half-circles.

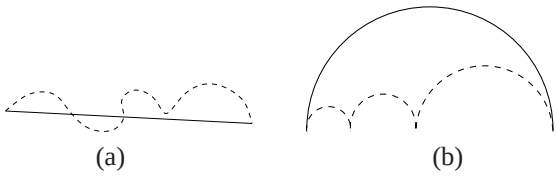

Figure 1. (a) Distance ratio is the ratio of the length of the curve (dashed line) to the distance between the two end points (solid line). (b) The two curves have the same distance ratio even though the dashed curve is more tortuous than the solid one.

Number of Inflection Points: An inflection point of a curve is the locus with zero curvature. For a curve specified by a series of points, the inflection point can be determined from the normal direction of a surface defined locally by a point P_k and its immediate neighborhoods P_{k-1} and P_{k+1}. Let $\mathbf{v}_1 = (P_k - P_{k-1})/|P_k - P_{k-1}|$ and $\mathbf{v}_2 = (P_{k+1} - P_k)/|P_{k+1} - P_k|$, then the normal $\mathbf{n}_k$ at P_k is the cross product

$$\mathbf{n}_k = \mathbf{v}_1 \times \mathbf{v}_2. \quad (1)$$

The normal $\mathbf{n}_{k+1}$ at P_{k+1} can be computed similarly using its neighbors P_k and P_{k+2}. If the curve segment at these four points bends in the same way, the two surface normals will be in the same direction, otherwise they will have opposite directions (Figure 2). If P_{k+2} is not in the plane determined by P_{k-1}, P_k and P_{k+1}, then $\mathbf{n}_k$ and $\mathbf{n}_{k+1}$ will not be exactly in the same or opposite directions. The inflection point can then be determined by identifying the local maxima in $|\nabla \mathbf{n}|$, where $\nabla \mathbf{n}$ can be computed as the difference of neighboring normal directions. A similar method in [1] determines an inflection point using the concept of Frenet frame [5].

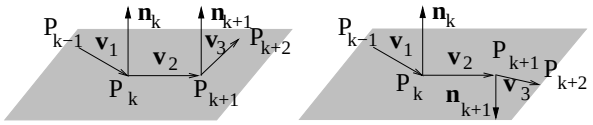

Figure 2. Inflection points: the normals are in the same direction at non-inflection points (left), and are in the opposite direction at inflection points (right).

Since a single arc and a straight line have no inflection point, they will report the same tortuosity of zero. One suggested measure combines the number of inflection points with the distance ratio: it adds one to the number of inflection points and multiplies the result by the distance ratio [1].

Sum of Angles: Any measures of curve tortuosity that combine the distance ratio and the number of inflection points cannot differentiate between an arc and a coil (Figure 3). This confusion can be solved by measuring the total angles of curvature [1]. At each P_k, the total angle (θ_k) is associated with two components : an in-plane angle (ρ_k) and a torsional angle (τ_k). They are computed using the inverse cosines of two dot products:

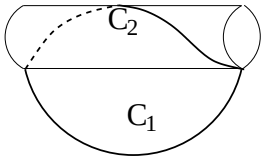

Figure 3. Suppose the arc (C_1) and the coil (C_2, formed by wrapping around a cylinder) have the same ending points and length. As they both have no inflection point, their tortuosities are the same for any measures that only involve the distance ratio and the number of inflection points.

$$\rho_k = \arccos(\mathbf{v}_1 \cdot \mathbf{v}_2), \quad (2)$$
$$\tau_k = \arccos(\mathbf{n}_k \cdot \mathbf{n}_{k+1}), \quad (3)$$

and the total angle $\theta_k = \sqrt{\rho_k^2 + \tau_k^2}$. The sum of the angles is $\sum_k \theta_k$. It is commonly divided by the length of the curve for normalization.

3. Measures of Surface Tortuosity

We propose measures of surface tortuosity based on the surface normal ($\mathbf{n}$) and the two principal curvatures (k_1, k_2). At each point on a smooth surface. these properties are defined in differential geometry [3] as follows: $\mathbf{n}$ is the normal direction of the tangent plane, and k_1, k_2 are the maximum and minimum curvatures of the set of curves crossing that point. This set of curves is formed at the intersection of the surface with a plane determined by the surface normal $\mathbf{n}$ and a vector $\mathbf{t}$ in the tangent plane (Figure 4).

These geometric quantities are often reformulated as a spatial average at each vertex for a piece-wise linear triangular mesh [7]. In order to do so, the surface patches of the mesh must form a *complex*: any two triangles either do not meet, or only meet at an edge or a vertex.

Average Angle between Surface Normals ($\mu_\theta^{\mathbf{n}}$): Similar to the sum of angles in measuring the curve tortuosity, we calculate the average of angles between every neighboring pairs of surface normals. We first compute, at every vertex i, the sum of angles between $\mathbf{n}_i$ and its neighbors $\{\mathbf{n}_{ij}\}$: $\theta_i =$

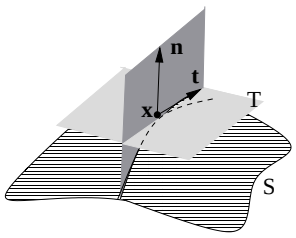

Figure 4. A curve formed as the intersection of the surface S with a plane determined by the normal vector $\mathbf{n}$ at $\mathbf{x}$, and a vector $\mathbf{t}$ on the tangent plane T.

$\sum_j \arccos(\mathbf{n}_i \cdot \mathbf{n}_{ij})$. Summing over all vertices will result in every angle between each pair of neighboring vertices being computed twice. Therefore, we define the average angle between surface normals as:

$$\mu_\theta^{\mathbf{n}} = \frac{1}{2N_e}\sum_i \theta_i = \frac{1}{2N_e}\sum_i\sum_j \arccos(\mathbf{n}_i \cdot \mathbf{n}_{ij}), \quad (4)$$

where N_e is the total number of edges. $\mu_\theta^{\mathbf{n}}$ will be zero on a flat surface (Figure 5 (a)) as the normals are everywhere identical. It will be within $(0, \pi]$ on a curved surface.

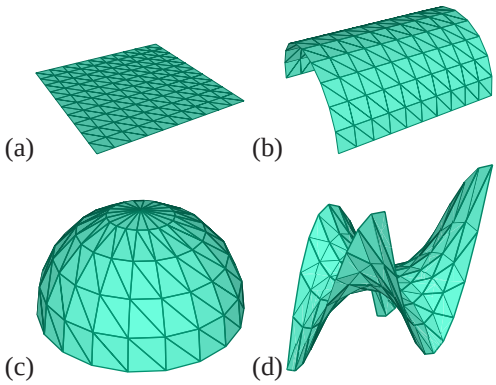

Figure 5. Surface properties are discussed on four types of simple geometric surfaces: (a) a flat surface, (b) a half cylinder, (c) a half sphere, and (d) a saddle surface.

Average Principal Curvatures (μ_{k_1}, μ_{k_2}): Some surfaces have distinctive properties of curvatures in different orientations. The curvature of a half cylinder (Figure 5 (b)) is positive along the circular direction and is zero along the lateral direction. A single measure of $\mu_\theta^{\mathbf{n}}$ will not fully characterize the properties of the surface. We compute two average principal curvatures by calculating the sums of maximum and minimum principal curvatures at every vertex, and dividing the sums by the number of vertices:

$$\mu_{k_1} = \frac{1}{N_v}\sum_i k_{1,i}, \quad (5)$$

$$\mu_{k_2} = \frac{1}{N_v}\sum_i k_{2,i}, \quad (6)$$

where N_v is the total number of vertices.

Standard Deviations of Principal Curvatures ($\sigma_{k_1}, \sigma_{k_2}$): Other than the average principal curvatures, we also compute the standard deviations as a measure of how "uniformly" k_1 and k_2 are distributed across the surface:

$$\sigma_{k_1} = \sqrt{\frac{1}{N_v}\sum_i (k_{1,i} - \mu_{k_1})^2}, \quad (7)$$

$$\sigma_{k_2} = \sqrt{\frac{1}{N_v}\sum_i (k_{2,i} - \mu_{k_2})^2}. \quad (8)$$

As the principal curvatures of the half cylinder and the half sphere (Figure 5 (c)) are identical everywhere, their corresponding standard deviations will be zero. Non-zero results are expected for the saddle surface in Figure 5 (d).

4. Results

We first examine the four types of simple geometric surfaces in Figure 5. Various measures of tortuosity are listed in Table 1. Every property of a flat surface is of value zero. The saddle is the most tortuous in terms of average angle. For the half cylinder, the difference between two principal curvatures is expected, while the small non-zero value in σ_{k_1} is caused by the limited mesh resolution. Although the principal curvatures are identical everywhere on a smooth spherical surface, there is some difference in the results of half sphere due to the uneven distribution of mesh vertices. In the saddle surface, the two principal curvatures have opposite signs. Their large standard deviations also indicate its sinuosity.

	$\mu_\theta^{\mathbf{n}}$	μ_{k_1}	σ_{k_1}	μ_{k_2}	σ_{k_2}
flat surface	0	0	0	0	0
half cylinder	0.19	0.21	0.05	0	0
half sphere	0.28	0.25	0.03	0.19	0.05
saddle surface	0.32	0.52	0.30	-0.52	0.30

Table 1. Results of various measures of tortuosity from four types of geometric surfaces.

We then apply these measures to the crack surface recovered from volumetric concrete images. The concrete sequence we use is composed of four images, B1, B2, B3 and

B4. The first image, B1, has no cracks. There are widening cracks in B2 through B4. The size of each image is $704 \times 768 \times 512$. The dimension of a voxel is $(6\mu m)^3$.

There are different numbers of cracks in each image. B2 has only one crack, B3 has five cracks, and B4 have eighteen cracks. The triangulated meshes of crack surfaces are displayed in Figure 6. A fixed set of colors is used. The color of a crack surface is determined by the rank in the number of its constituent triangles.

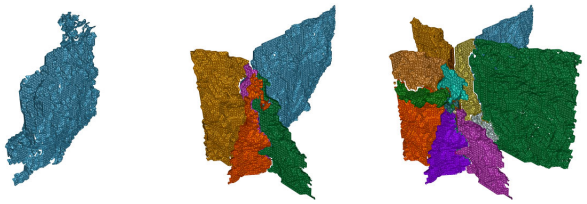

Figure 6. Crack surfaces in B2, B3, and B4.

The various measures on these crack surfaces are listed in Table 2. All cracks in B2 and B3 are included in the table, but only the largest ten cracks of B4 are listed due to the limited space. Despite their different sizes and locations, all cracks have similar values in every measure. Compared with the saddle surface, the cracks also have relatively large values in $\mu_\theta^{\mathbf{n}}$, and opposite signs in μ_{k_1}, μ_{k_2}. However, the values are much smaller than those of the saddle surface. This indicates that the crack surfaces have bumps and dents, but their amplitudes are much smaller. This can be observed by comparing the pictures directly.

Comparing the amplitude of the principal curvature with that of the corresponding standard deviation, it is also observed that the former is larger for geometric surfaces, while the latter is larger for the crack surfaces. This can be explained by the geometric surfaces still being quite smooth despite some surface irregularity, while the crack surfaces having many bumps and dents.

5. Conclusion

We have derived several measures of surface tortuosity based on surface normals and principal curvatures. We demonstrate that these measures can differentiate some simple geometrical surfaces. We have also applied these measures to analyze the crack surfaces recovered from volumetric image sequences. The results show that (1) the crack surfaces of concrete are locally tortuous with bumps and dents, but they are still quite "flat" globally; (2) the crack surfaces, despite their different sizes and spatial locations, have very similar properties in surface tortuosity.

Acknowledgments: The authors wish to thank Prof. Eric Landis for providing the volumetric concrete images.

	$\mu_\theta^{\mathbf{n}}$	μ_{k_1}	σ_{k_1}	μ_{k_2}	σ_{k_1}
B2	0.42	0.030	0.046	-0.033	0.046
B3	0.35	0.023	0.032	-0.023	0.032
	0.36	0.022	0.034	-0.026	0.036
	0.34	0.021	0.030	-0.026	0.033
	0.37	0.027	0.039	-0.026	0.035
	0.32	0.021	0.027	-0.023	0.030
B4	0.35	0.022	0.031	-0.022	0.031
	0.37	0.026	0.035	-0.024	0.035
	0.37	0.025	0.033	-0.023	0.032
	0.36	0.021	0.031	-0.027	0.034
	0.37	0.023	0.033	-0.028	0.034
	0.37	0.020	0.034	-0.030	0.038
	0.42	0.025	0.040	-0.038	0.048
	0.34	0.023	0.029	-0.024	0.033
	0.33	0.021	0.027	-0.025	0.031
	0.45	0.025	0.044	-0.041	0.047

Table 2. Results of various measures of tortuosity on the crack surfaces in the 3D images of B2, B3, and B4.

References

[1] E. Bullitt, G. Gerig, S. Pizer, W. Lin, and S. Aylward. Measuring tortuosity of the intracerebral vasculature from mra images. *IEEE Transactions on Medical Imaging*, 22(9):1163–1171, Sept. 2003.

[2] E. Garboczi, D. Bentz, and G. Frohnsdorff. The past, present, and future of the computational materials science of concrete. In *Proceedings of the J. Francis Young Symposium (Materials Science of Concrete Workshop)*, Lake Shelbyville, IL, April 27-29 2000.

[3] A. Gray. *Modern Differential Geometry of Curves and Surfaces with Mathematica*. CRC Press, 2nd edition, 1997.

[4] W. Hart, M. Goldbaum, B. Cote, P. Kube, and M. R. Nelson. Measurement and classification of retinal vascular tortuosity. *International Journal of Medical Informatics*, 53:239–267, 1999.

[5] J. J. Koenderink. *Solid shape*. MIT Press, Cambridge, Mass., 1990.

[6] E. N. Landis, E. N. Nagy, D. T. Keane, and G. Nagy. Technique to measure 3d work-of-fracture of concrete in compression. *Journal of Engineering Mechanics*, 125(6):599–605, June 1999.

[7] M. Meyer, M. Desbrun, P. Schröder, and A. H. Barr. *Visualization and Mathematics III*, chapter 2, pages 35–57. Springer-Verlag, Heidelberg, 2003.

[8] D. A. Rusakov and D. M. Kullmann. Geometric and viscous components of the tortuosity of the extracellular space in the brain. *Proc. Natl. Acad. Sci. USA*, 95:8975–8980, July 1998.

[9] J. van Mier. *Fracture Processes of Concrete*. CRC Press, New York, 1997.

[10] T. Zhang. *Identification of Structural Changes from 3D Volumetric Image Sequence*. PhD thesis, Rensselaer Polytechnic Institute, May 2004.